AMERICAN SOCIETY FOR MICROBIOLOGY | Antimicrobial Agents and Chemotherapy®

MECHANISMS OF RESISTANCE

Genetic and Transcriptomic Analyses of Ciprofloxacin-Tolerant *Staphylococcus aureus* Isolated by the Replica Plating Tolerance Isolation System (REPTIS)

Miki Matsuo,[a] Miyu Hiramatsu,[b] Madhuri Singh,[c] Takashi Sasaki,[d] Tomomi Hishinuma,[a] Norio Yamamoto,[b] Yuh Morimoto,[e] Teruo Kirikae,[a] Keiichi Hiramatsu[e]

[a]Department of Microbiology, Faculty of Medicine, Juntendo University, Tokyo, Japan
[b]Department of Infection Control Science, Graduate School of Medicine, Juntendo University, Tokyo, Japan
[c]School of Environmental Sciences, Jawaharlal Nehru University, New Delhi, India
[d]Animal Research Center, Sapporo Medical University School of Medicine, Sapporo, Japan
[e]Research Centre for Infection Control Science, Juntendo University, Tokyo, Japan

ABSTRACT We developed a simple, efficient, and cost-effective method, named the replica plating tolerance isolation system (REPTIS), to detect the antibiotic tolerance potential of a bacterial strain. This method can also be used to quantify the antibiotic-tolerant subpopulation in a susceptible population. Using REPTIS, we isolated ciprofloxacin (CPFX)-tolerant mutants (mutants R2, R3, R5, and R6) carrying a total of 12 mutations in 12 different genes from methicillin-sensitive *Staphylococcus aureus* (MSSA) strain FDA209P. Each mutant carried multiple mutations, while few strains shared the same mutation. The R2 strain carried a nonsense mutation in the stress-mediating gene, *relA*. Additionally, two strains carried the same point mutation in the *leuS* gene, encoding leucyl-tRNA synthetase. Furthermore, RNA sequencing of the R strains showed a common upregulation of *relA*. Overall, transcriptome analysis showed downregulation of genes related to translation; carbohydrate, fat, and energy metabolism; nucleotide synthesis; and upregulation of amino acid biosynthesis and transportation genes in R2, R3, and R6, similar to the findings observed for the FDA209P strain treated with mupirocin (MUP0.03). However, R5 showed a unique transcription pattern that differed from that of MUP0.03. REPTIS is a unique and convenient method for quantifying the level of tolerance of a clinical isolate. Genomic and transcriptomic analyses of R strains demonstrated that CPFX tolerance in these *S. aureus* mutants occurs via at least two distinct mechanisms, one of which is similar to that which occurs with mupirocin treatment.

KEYWORDS *Staphylococcus aureus*, ciprofloxacin tolerance, *leuS*, *relA*, tolerant mutant, transcriptome

Increasing ciprofloxacin (CPFX) resistance among urinary tract infection (UTI) pathogens, such as *Escherichia coli*, has led to reconsideration of the continuation of CPFX as an empirical therapy against UTIs (1). CPFX is also prescribed for *Staphylococcus aureus* infections, especially those caused by methicillin-resistant *Staphylococcus aureus* (MRSA) strains. However, 80% of hospital-acquired MRSA strains have been found to be CPFX resistant (2–4). Moreover, CPFX resistance in *S. aureus* has genetically evolved through the acquisition of mutations in the *gyrA* gene (2, 5, 6) or the *norA* gene (7). Both the resistance and the tolerance of *S. aureus* to antibiotics cause therapeutic failure by inducing persister cell formation (8). However, we have no information on the prevalence of antibiotic tolerance among clinical isolates of *S. aureus*.

Unlike resistant mutants, which show increased MICs, tolerance is the ability of a cell

Citation Matsuo M, Hiramatsu M, Singh M, Sasaki T, Hishinuma T, Yamamoto N, Morimoto Y, Kirikae T, Hiramatsu K. 2019. Genetic and transcriptomic analyses of ciprofloxacin-tolerant *Staphylococcus aureus* isolated by the replica plating tolerance isolation system (REPTIS). Antimicrob Agents Chemother 63:e02019-18. https://doi.org/10.1128/AAC.02019-18.

Copyright © 2019 American Society for Microbiology. All Rights Reserved.

Address correspondence to Miki Matsuo, mmatsuo@juntendo.ac.jp.

Received 20 September 2018
Returned for modification 16 October 2018
Accepted 21 November 2018
Accepted manuscript posted online 3 December 2018
Published 29 January 2019

Downloaded from https://journals.asm.org/journal/aac on 24 February 2022 by 2a01:4f9:3b:1ae9::

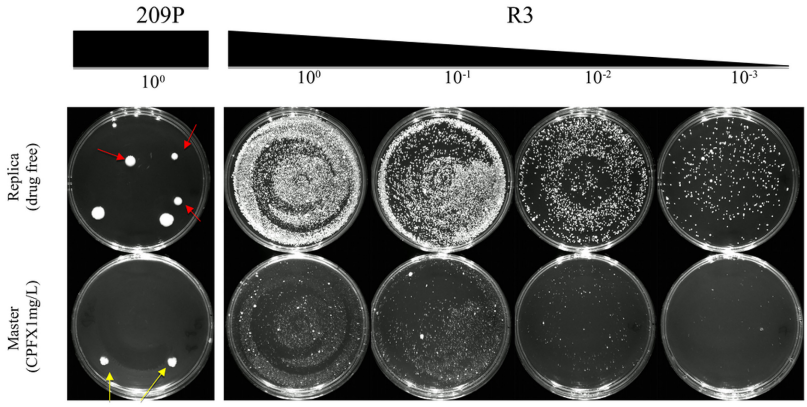

FIG 1 Determining *S. aureus* tolerance to CPFX using the replica plating tolerance isolation system (REPTIS). The number of surviving cells following CPFX (1 mg/liter) treatment is greater for the R3 mutant than for the parent FDA209P strain. FDA209P (10^8 CFU) was exposed to CPFX at 1 mg/liter on an agar plate, while different initial inocula (10^8, 10^7, 10^6, and 10^5 CFU) of R3 were exposed to CPFX. Red arrows, tolerant colonies; yellow arrows, resistant colonies.

subpopulation to survive transient exposure to antibiotics without altering the MIC (9). However, a heteroresistant strain contains cell subpopulations with different levels of antibiotic resistance (10). The mechanism of tolerance is completely different from that of resistance (11–14). For example, quinolone persistence in *S. aureus* is attributed to a decrease in ATP levels (8). The same antibiotics that kill susceptible cells by targeting active metabolic processes (15) are unlikely to kill tolerant variants with a reduced metabolism (16). Therefore, it is not surprising that even strains with antibiotic MICs below susceptibility breakpoints can be drug tolerant, as previously shown by our group (13) and others (12).

Although antibiotic tolerance has been noted since the discovery of antibiotics in the 1940s, researchers have been unable to decipher the genetic basis of tolerance due to limited experimental methods for distinguishing tolerant, heteroresistant, and resistant mutants (17). Tolerance is the main cause of relapse of bacterial infections and also promotes the eventual evolution of overt antibiotic resistance (18). Therefore, development of a simple method to isolate tolerant strains and to identify their molecular targets is needed. Such a method will subsequently enable the design of drugs to eradicate persistent infections. Several attempts have been made to solve the mysteries of antibiotic tolerance, particularly by isolating and quantifying tolerant variants from a heterogeneous population, yet none have been simple or cost-effective enough for use in clinics on a routine basis (11, 19–21).

Here, we developed a replica plating method, called the replica plating tolerance isolation system (REPTIS), to simplify the isolation and differentiation of tolerant mutants from resistant mutants. As a proof of concept, we isolated CPFX-tolerant mutants from methicillin-sensitive *S. aureus* (MSSA) strain FDA209P. Using REPTIS, we successfully selected four *S. aureus* mutants exhibiting the CPFX tolerance phenotype and further confirmed their CPFX tolerance phenotype in comparison to the sensitive phenotype of the parent strain, as well as other hallmarks of tolerance, such as slow growth and a reduced killing rate (22–24). These four CPFX-tolerant strains were then analyzed for genetic and physiological alterations from the parent FDA209P strain using whole-genome sequencing and RNA sequencing (RNA-seq).

RESULTS

Evolution of strains with high CPFX tolerance from MSSA using REPTIS. When approximately 10^8 CFU of FDA209P cells was inoculated onto an agar plate and incubated for 48 h in the presence of 1 mg/liter CPFX (a concentration 15-fold higher than the MIC), no colonies were visible, with the exception of a few resistant colonies growing in the presence of CPFX (Fig. 1). However, if tolerant bacteria exist, then other

Downloaded from https://journals.asm.org/journal/aac on 24 February 2022 by 2a01:4f9:3b:1ae9::

TABLE 1 Summary of the rate of survivors in the presence of CPFX for the four tolerant mutants based on REPTIS

Strain	No. of input cells (no. of CFU/master plate)	No. of colonies (no. of CFU/replica plate)	Ratio of survivors	
			Total	Mutant/parent
FDA209P	6.8×10^8	2.5×10^1	3.7×10^{-8}	
R2	9.4×10^8	5.7×10^2	6.1×10^{-7}	1.7×10^1
R3	2.9×10^8	2.7×10^6	9.2×10^{-3}	2.5×10^5
R5	1.3×10^7	1.8×10^5	1.4×10^{-2}	3.9×10^5
R6	6.3×10^8	2.0×10^4	3.2×10^{-5}	8.7×10^2

surviving cells must be present on the plate. Therefore, we transferred all colonies from the CPFX plate, including both resistant and tolerant cells (i.e., cells not growing in the presence of CPFX and, thus, not visible on the CPFX plate) onto a drug-free plate (the replica plate) using replica plating. After incubating the replica plate for 3 days, six very small colonies appeared (Fig. 1). All colonies grew extremely slowly, and four colonies from duplicate experiments were purified and stored for further analyses. These strains were designated R2, R3, R5, and R6, and each of these surviving strains showed a higher ratio of survivors in the presence of CPFX than the parent FDA209P strain (Table 1). Figure 1 shows a representative image of the increased tolerance of R3, which had a 2.5×10^5-fold higher proportion of survivors in the presence of CPFX (1 mg/liter) than the parent FDA209P strain (Table 1). As expected, after incubation on a plate with 1 mg/liter CPFX, R3 had more than 10,000 times as many survivors as the parent strain. Similarly, the R2, R5, and R6 strains had a 1.7×10^1-, 3.9×10^5-, and 8.7×10^2-fold higher ratio of the number of survivors relative to the number of survivors of the parent FDA209P strain, respectively (Table 1). In summary, the easy-to-use and cost-effective REPTIS method enabled the successful identification of tolerant mutants and quantification of the relative proportion of tolerance. Next, we analyzed the phenotypic and genotypic characteristics of these four R strains.

CPFX-tolerant phenotypes of the mutant strains. First, we determined the CPFX MIC of the FDA209P-derived survivor strains using an Etest. Although the MIC of each of the four evolved strains was slightly increased compared to that of the parent strain (0.064 mg/liter), all of the MIC values were $\leq$0.19 mg/liter (Table 2), which is below the CPFX susceptibility breakpoint of 1 mg/liter.

By definition, a typical tolerant strain shows an increase in the minimum duration required to kill 99.9% of the cell population ($MDK_{99.9}$) compared to that for the parent strain (22). The CPFX-induced killing levels of the evolved strains were compared with those of the parent FDA209P strain. The killing activity of CPFX (1 mg/liter) against all mutants was clearly reduced and slower than that against the parent FDA209P strain (Fig. 2a to d). After treatment with CPFX for 24 h, the ratio of surviving cells was $\geq$0.01 for all R strains, which was much higher than that for the parent FDA209P strain (0.000089). Using the killing curves, the estimated $MDK_{99.9}$ for FDA209P was 11.7 h, whereas it was >24 h for all R strains. These R strains were also tolerant to vancomycin (data not shown).

Next, we measured the growth rate and lag time of the CPFX-tolerant strains relative to those of FDA209P. All of the mutant strains (R2, R3, R5, and R6) had an extremely

TABLE 2 MIC of ciprofloxacin, doubling time, and lag time of the FDA209P-derived tolerant strains

Strain	Doubling time (min)	Lag time (h)	MIC[a] (mg/liter)	$MDK_{99.9}$[b] (h)
FDA209P	37	12	0.064	12
R2	94	21	0.13	>24
R3	145	35	0.13	>24
R5	92	24	0.19	>24
R6	122	25	0.19	>24

[a]The MIC was determined using an Etest and incubation for 48 h at 37°C.
[b]$MDK_{99.9}$, minimum duration required to kill 99.9% of the cell population.

Downloaded from https://journals.asm.org/journal/aac on 24 February 2022 by 2a01:4f9:3b:1ae9::

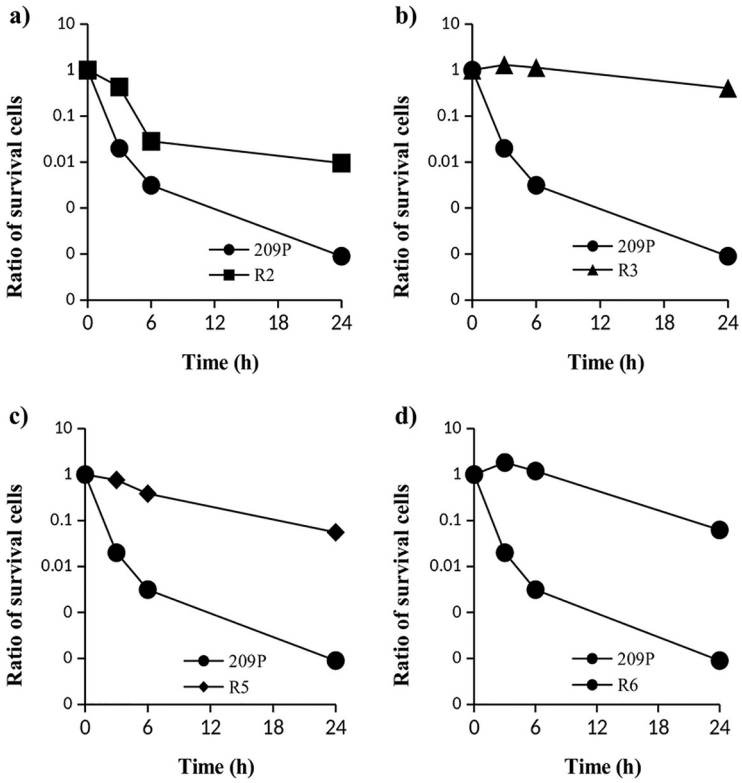

FIG 2 Time-kill assay of the strains surviving exposure to CPFX compared to the parent FDA209P strain. The killing kinetics of the R2 (a), R3 (b), R5 (c), and R6 (d) strains compared to those of the parent FDA209P strain in the presence of CPFX (1 mg/liter) are shown. Data are presented as the mean ± SD from three independent experiments.

long doubling time (94, 145, 92, and 122 min, respectively) compared to that of the parent FDA209P strain (37 min) (Table 2). These mutants also exhibited a significant delay in regrowth after exposure to 1 mg/liter CPFX, with a prolonged lag phase (from 21 to 35 h) compared to that for FDA209P (12 h).

Identification of mutations in CPFX-tolerant strains. To clarify the genetic basis of CPFX tolerance, the whole-genome sequences of the tolerant strains were compared to the whole-genome sequence of the parental FDA209P strain. As listed in Table 3, a total of 12 mutations in 12 genes were identified in these strains. Each of the strains carried a different mutation set, with the exception of a missense mutation in the *leuS* gene, which encodes leucyl-tRNA synthetase and which was present in both R5 and R6. R5 also had a missense mutation (A385G) in the SAFDA_2343 gene, encoding phosphoglucomutase, and two insertion mutations in the genes *fruB* and *ilvB*, which encode fructose 1-phosphate kinase and the acetolactate synthase large subunit, respectively. R6 carried two insertion mutations, one in the *murC* gene, encoding UDP-*N*-acetylmuramate-L-alanine ligase, and another insertion frameshift mutation in *vga*, encoding an ABC transporter ATPase, which introduces a premature stop codon. The R3 strain carried three insertion mutations in three different genes: a single amino acid insertion in *secA*, encoding a preprotein translocase subunit, and two frameshift mutations in the *ecsA* homolog and *mqo-2* genes, which encode an ABC transporter ATPase and malate dehydrogenase, respectively. R2 had a missense mutation (T114I) in *tkt*, encoding transketolase, and a nonsense mutation at position 360 in the *relA* gene, which encodes the GTP pyrophosphokinase RelA. Importantly, *S. aureus* RelA contains guanosine tetra(penta)phosphate [(p)ppGpp] synthetase and hydrolase domains in its N-terminal region and a regulatory domain in its C-terminal region (25). The nonsense mutation in R2 (Q360*) was located between the synthetase and regulatory domains, suggesting that the RelA regulatory region was deleted in this mutant.

Downloaded from https://journals.asm.org/journal/aac on 24 February 2022 by 2a01:4f9:3b:1ae9::

TABLE 3 Mutation sites identified in the mutant strains

					Nucleotide changes			Amino acid changes			
Strain	ORF identifier	Gene	Gene product	Type	Position(s)	Parent	Mutant	Position(s)	No. of amino acids in parent	Parent	Mutant
R2	SAFDA_1239	*tkt*	Transketolase	SNV[a]	1330342	C	T	114	662	T	I
	SAFDA_1529	*relA*	GTP Pyrophosphokinase	SNV	1659937	G	A	360	729	Q	[b]
	SAFDA_2387	HP[c]	Permease of the drug/metabolite transporter (DMT) superfamily	Insertion, frameshift	2573982,[d] 2573983		C	238	308	A	ATRILFLYRQFTIHISERNNIIRNC[b]
R3	SAFDA_0697	*secA*	Preprotein translocase subunit	Insertion	779357,[d] 779358		CGG	272,[d] 273	843		A
	SAFDA_1725	ecsA homolog	ABC transporter ATPase	Deletion, frameshift	1879939,[e] 0.1879940	AT		103	246	Y	
	SAFDA_2460	*mqo-2*	Malate dehydrogenase	Insertion, frameshift	2648331,[d] 2648332		AGTTTTGT	457	498	E	TKLNGHLKSRK[b]
R5	SAFDA_0645	*fruB*	Fructose 1-phosphate kinase	Insertion	719558,[d] 719559		TATGCG	146,[d] 147	306		TA
	SAFDA_1645	*leuS*	Leucyl-tRNA synthetase	SNV	1804163	G	A	422	804	R	C
	SAFDA_1928	*ilvB*	Acetolactate synthase large subunit	Insertion	2080723,[d] 2080724		ACGGAT	118,[d] 119	589		TD
	SAFDA_2343	HP	Phosphomannomutase	SNV	2522794	A	G	385	583	Y	C
R6	SAFDA_1627	*murC*	UDP-*N*-acetylmuramate-L-alanine ligase	Insertion	1777256,[d] 1777257		CATCCA	248,[d] 249	473		VD
	SAFDA_1645	*leuS*	Leucyl-tRNA synthetase	SNV	1804163	G	A	422	804	R	C
	SAFDA_1920	*vga*	ABC transporter ATPase	Insertion, frameshift	2072009,[d] 2072010		GGTTA	340	642	Y	[b]

[a]SNV, single nucleotide variation.
[b]Stop codon.
[c]HP, hypothetical protein.
[d]Insertion site.
[e]Deletion site.

Downloaded from https://journals.asm.org/journal/aac on 24 February 2022 by 2a01:4f9:3b:1ae9::.

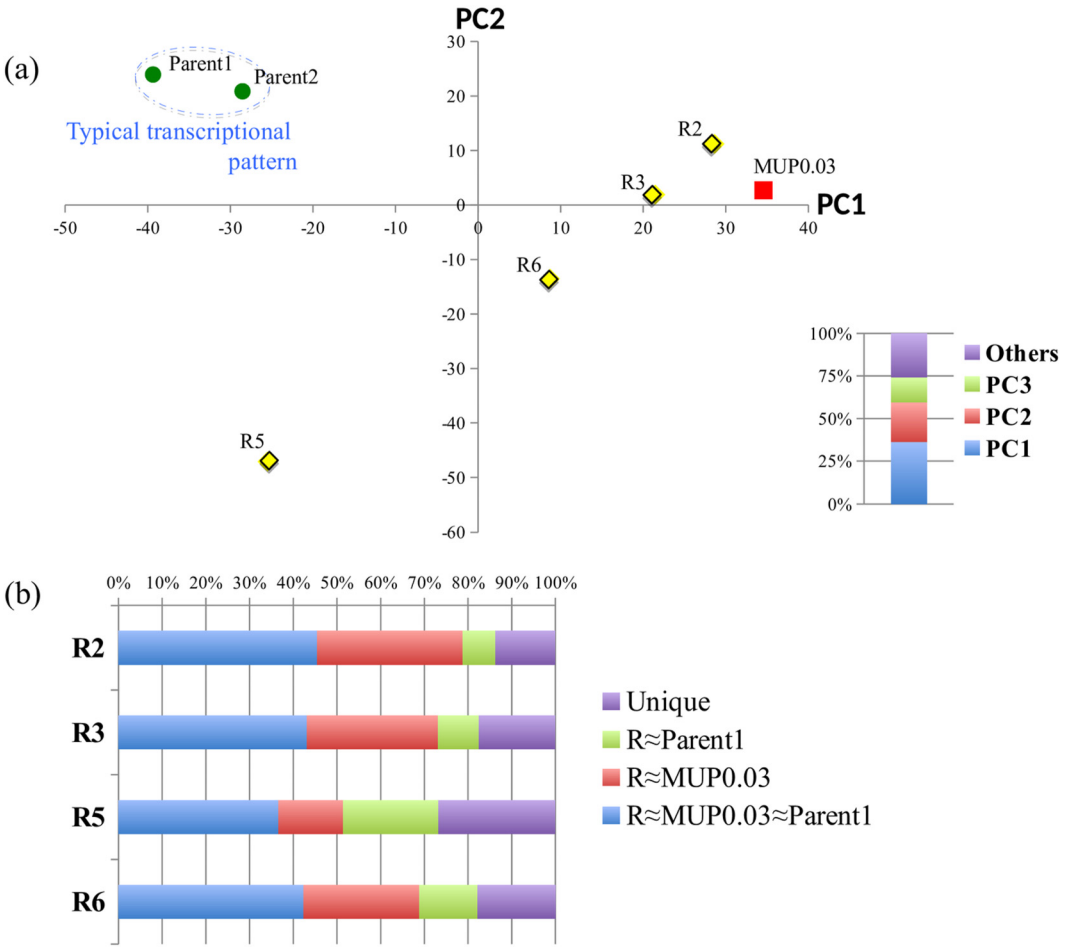

FIG 3 Global gene expression analysis of CPFX-tolerant mutants compared to FDA209P treated or not treated with mupirocin. (a) Principal-component analysis (PCA) of whole-genome expression. The gene expression pattern of three of the four CPFX-tolerant strains (R2, R3, and R6) was similar to that of mupirocin-treated FDA209P (MUP0.03), while the transcriptome of R5 was unique. (b) Comparison of whole-genome regulation among the CPFX-tolerant mutants (R) versus MUP0.03 and parent strain FDA209P. The expression patterns are classified into four types: R ≈ MUP0.03 ≈ parent1 (conserved), R ≈ MUP0.03 (stringent pattern), R ≈ parent1 (unchanged), or unique.

Analysis of global gene expression by RNA sequencing. To gain a further understanding of the cellular pathways involved in CPFX tolerance in *S. aureus*, we compared the transcriptomes of R mutants to the transcriptome of the parent FDA209P strain grown under normal conditions (Fig. 3 and 4). In addition, the transcriptome of FDA209P cells treated with mupirocin at a sub-MIC (0.03 mg/liter) was also examined to determine the correlation between CPFX tolerance and the stringent response (SR) (26). The RNA sequencing experiments were performed in triplicate, and the results of transcriptome analysis in the present study were reproducible (see Fig. S1 in the supplemental material).

Principal-component analysis (PCA) was performed to predict the transcriptome pattern across the strains. As shown in Fig. 3a, the transcriptional patterns of three of the four R strains (R2, R3, and R6) were similar to the transcriptional pattern of mupirocin-treated FDA209P (referred as MUP0.03). However, the R5 mutant exhibited a unique transcriptional pattern, which was substantially different from that of MUP0.03 in both PC1 and PC2. Furthermore, the whole-genome expression of each of the R strains compared with that of mupirocin-treated FDA209P (MUP0.03) and FDA209P was categorized into four types, R ≈ MUP0.03 ≈ parent1 (conserved), R ≈ MUP0.03 (stringent pattern), R ≈ parent1 (unchanged), or unique, as illustrated in Fig. 3b. The pattern for R2 was the closest to that for MUP0.03, with the two strains expressing a

Downloaded from https://journals.asm.org/journal/aac on 24 February 2022 by 2a01:4f9:3b:1ae9::.

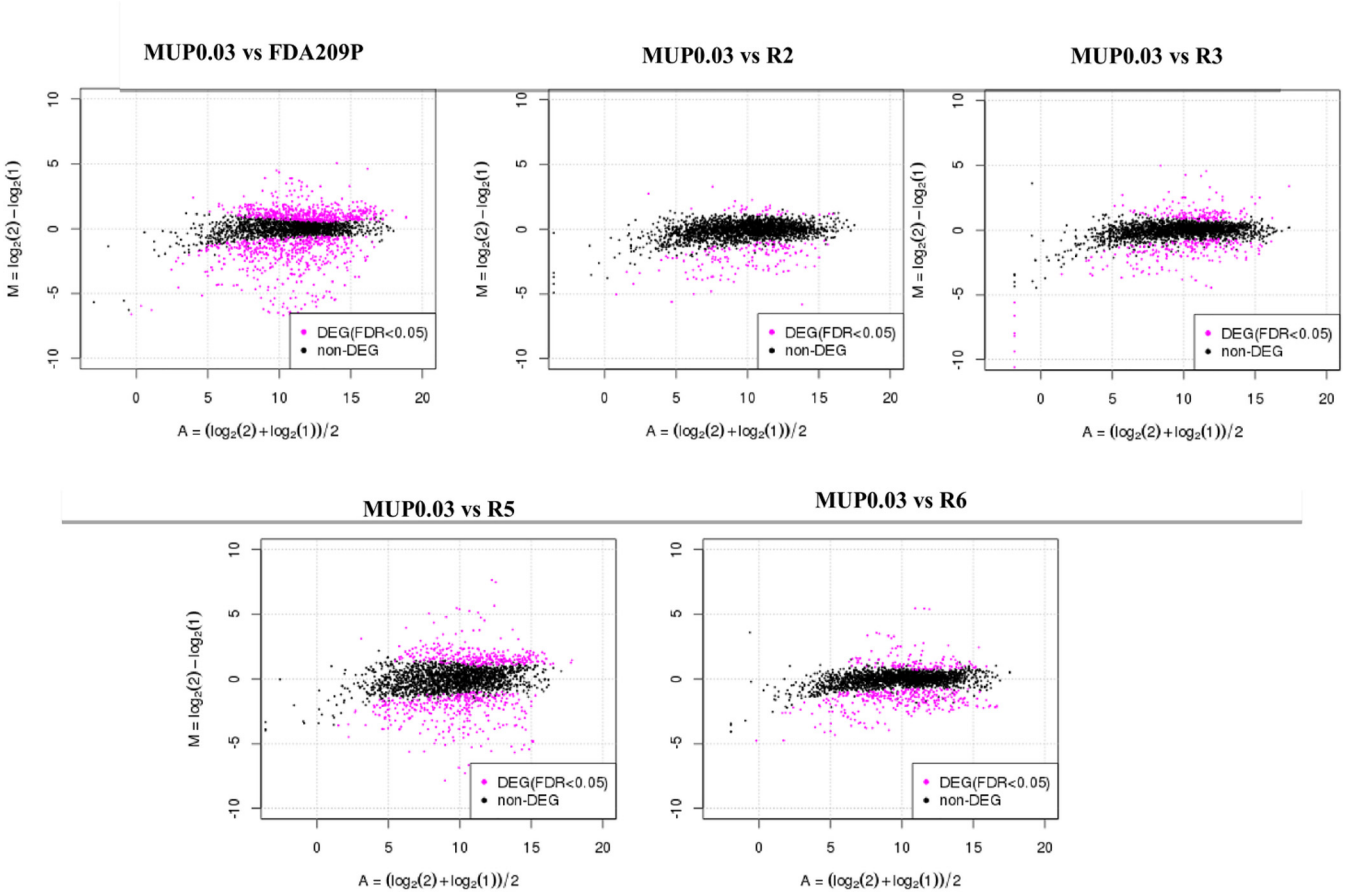

FIG 4 MA plots showing the relationship between mean expression and the fold change in expression for all genes. Dots represent individual genes. Black dots, non-differentially expressed genes; pink dots, differentially expressed genes (FDR threshold, <0.05).

similar maximum number of genes ($n = 855$). However, only 380 genes in R5 belonged to the stringent transcription pattern, and these were similar to those regulated in MUP0.03.

Similarly, MA plots of the MUP0.03 versus R strains (Fig. 4) showed that the mean gene expression of the differentially expressed genes (DEGs) among the R2, R3, and R6 strains corresponded to the gene expression in MUP0.03, while the mean expression values for DEGs in R5 were more disperse than those for DEGs in MUP0.03. These results indicate that gene expression in R5 deviated from that in the other R strains, as well as cells under stringent conditions.

Differential expression of genes in CPFX-tolerant strains and untreated FDA209P. Genes in each of the CPFX-tolerant mutants and in MUP0.03 cells that were down- or upregulated compared to their expression in the untreated parent FDA209P strain were grouped according to KEGG pathway categories, as shown in Fig. 5a and b, Fig. S2, and Table S1 (for FDA209P versus MUP0.03 and the R mutants). As described above, the global transcriptional pattern of R2, R3, and, to some extent, R6 was closer to that of MUP0.03, whereas R5 showed unique gene regulation. As illustrated in Fig. 5a, similar to the findings for MUP0.03, the majority of downregulated genes in R2, R3, and R6 were related to translation, particularly those located in the *rps* and *rpl* operons for ribosomal proteins. However, translation genes were marginally affected or unchanged in R5. The second highest proportion of downregulated genes were involved in general metabolic processes, including carbohydrate, nucleotide, fatty acid, and amino acid metabolic pathways, which were downregulated in all four R mutants as well as MUP0.03 (Fig. S2). Similarly, oxidative phosphorylation genes, such as ATP synthase genes (*atpABCDEFG*), were downregulated, while operons of nitrate reductase

Downloaded from https://journals.asm.org/journal/aac on 24 February 2022 by 2a01:4f9:3b:1ae9::

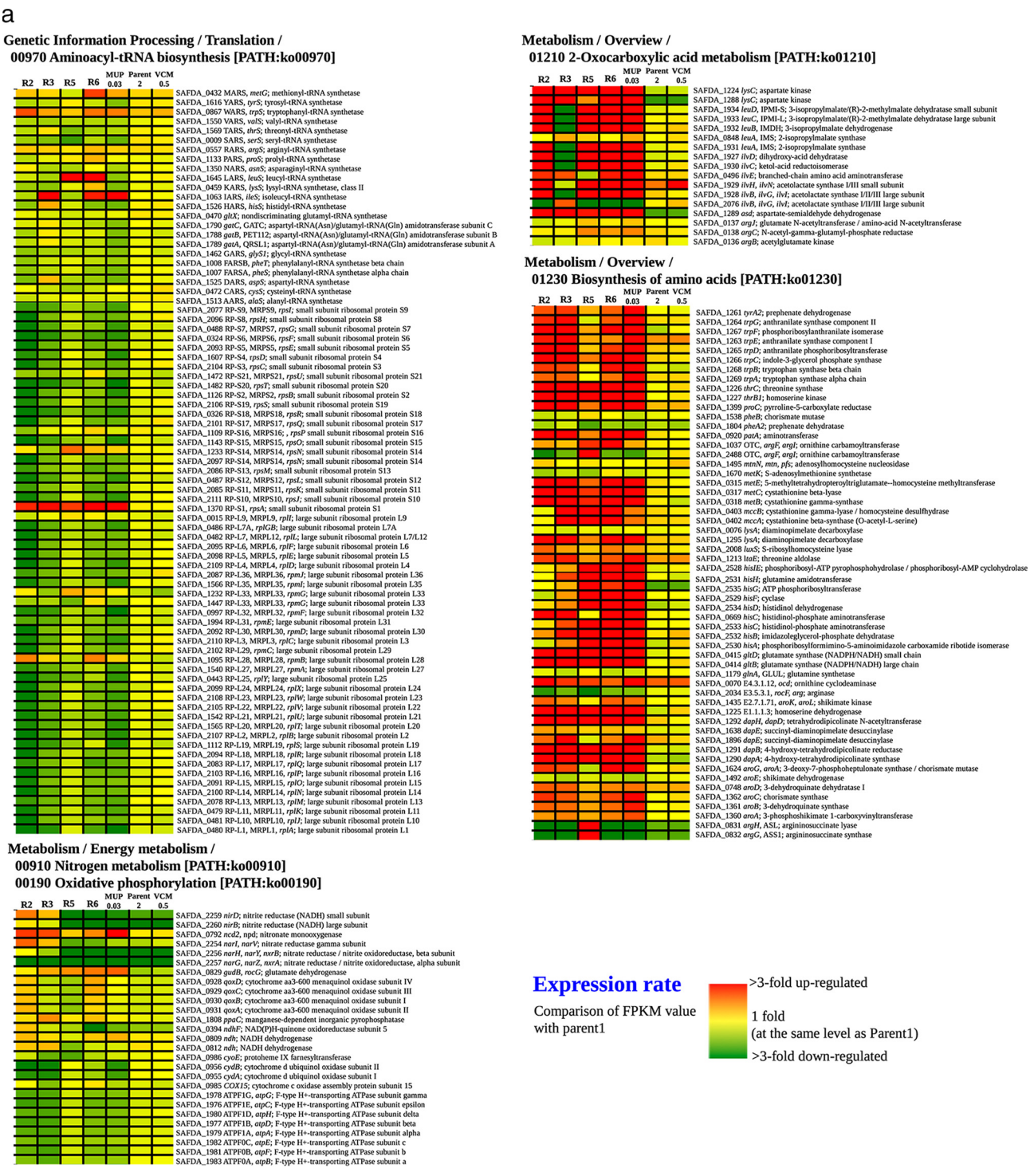

FIG 5 Heat map of the expression rate of the CPFX-tolerant R and MUP0.03 strains compared to that of the reference strain FDA209P (parent1). The expression rate of all strains compared to that of the parent1 strain is presented using a red-yellow-green gradient, with green indicating the bottom score (>3-fold downregulation) and red indicating the top score (>3-fold upregulation). These data represent the fold change in FPKM values compared to the corresponding gene expression in reference strain FDA209P (parent1). The categorization of differentially expressed genes is based on the KEGG pathway. (a) Genetic information processing/translation/aminoacyl-tRNA biosynthesis (PATH:ko00970), metabolism/energy metabolism/nitrogen metabolism (PATH:ko00910), metabolism/energy metabolism/oxidative phosphorylation (PATH:ko00190), metabolism/overview/2-oxocarboxylic acid metabolism (PATH:ko01210), and metabolism/overview/biosynthesis of amino acids (PATH:ko01230). (b) Environmental information processing/signal transduction/two-component system (PATH:ko02020) and environmental information processing/membrane transport/ABC transporters (PATH:ko02010), human diseases/infectious diseases/Salmonella infection (PATH:ko05132), human diseases/infectious diseases/epithelial cell signaling in Helicobacter pylori infection (PATH:ko05120), and human diseases/infectious diseases/bacterial invasion of epithelial cells (PATH:ko05100). A PATH number represents an entry code in the KEGG pathway database. The genes in this heat map correspond to the genes listed in Table S1 in the supplemental material. MUP, mupirocin; VCM, vancomycin.

Downloaded from https://journals.asm.org/journal/aac on 24 February 2022 by 2a01:4f9:3b:1ae9::

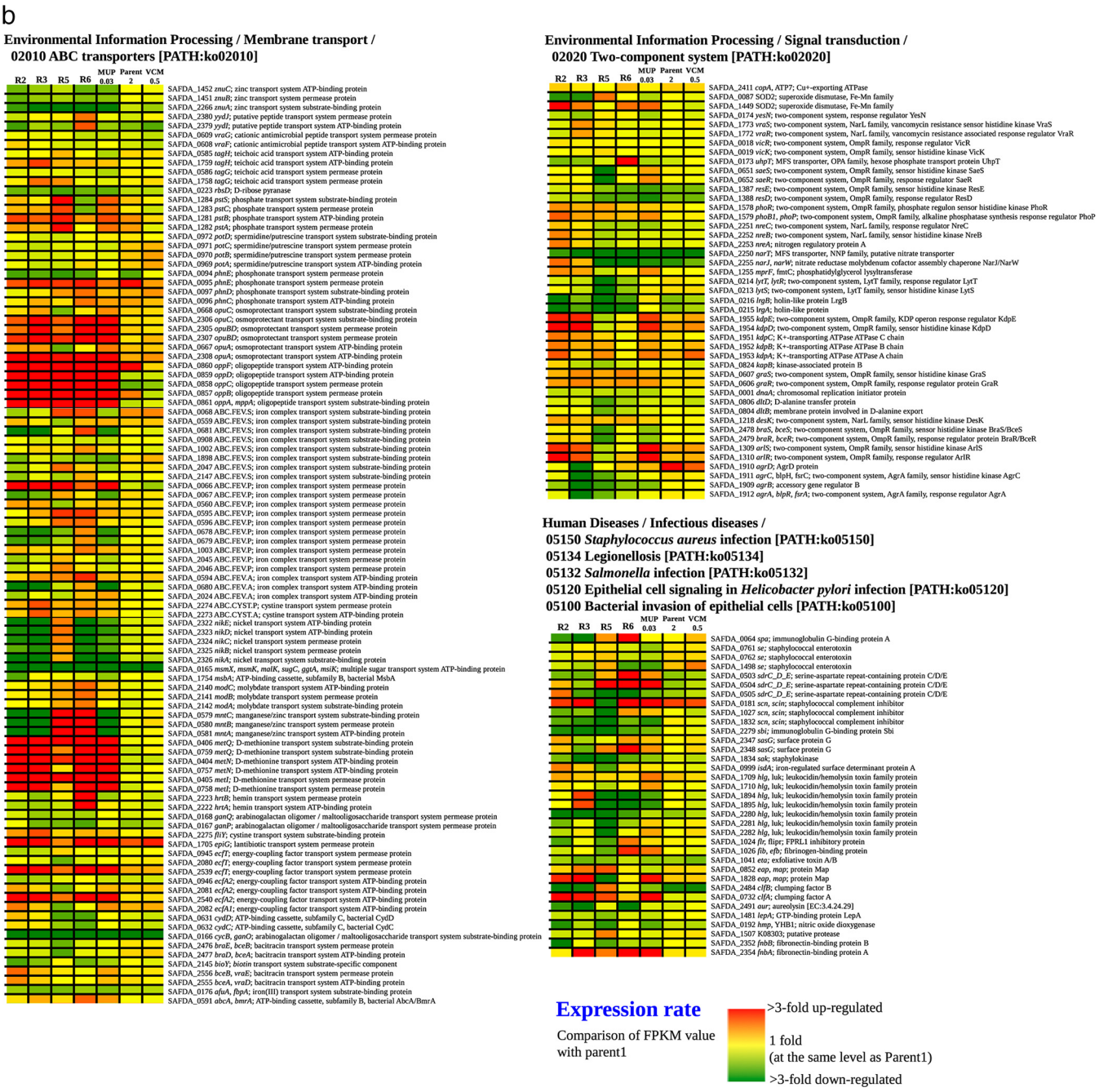

FIG 5 (Continued)

were upregulated (Fig. 5a). This expression pattern suggests that all CPFX-tolerant R strains and MUP0.03 cells were dependent on anaerobic respiration. Previously, the *narGHKI* operon, encoding nitrate reductase, was found to be upregulated in virulent *S. aureus* strains *in vivo* (27). Conversely, signal transduction genes, such as *agrABCD*, were significantly downregulated in R3 and R5, but their expression was unchanged in R2, R6, and MUP0.03 cells (Fig. 5b).

The largest proportion of upregulated genes were associated with amino acid biosynthesis and the ABC transport system, which were upregulated in all R strains, as in MUP0.03 (Fig. 5a and b). Notably, almost all operons related to amino acid biosynthesis were upregulated under mupirocin treatment conditions (MUP0.03); however, the R strains showed variable regulation of amino acid biosynthesis pathway-encoding

Downloaded from https://journals.asm.org/journal/aac on 24 February 2022 by 2a01:4f9:3b:1ae9::

operons. For example, all R strains showed the upregulation of the tryptophan (*trpAB-CDEFG*), tyrosine, methionine (*metABCD*), lysine (*lysAC* and *dapABDE*), and histidine (*hisABC*) biosynthesis pathways. Expression of the *ilv-leu* operon-encoding genes, required for the synthesis of branched-chain amino acids (BCAA), including isoleucine, leucine, and valine, was also substantially upregulated in the R2, R6, and R5 strains, similar to the findings for MUP0.03 (Fig. 5a). However, the *ilv-leu* operon was downregulated 8- to 10-fold in R3 (Table S1). Additionally, virulence genes, such as clumping factor genes (*clfAB*) and fibrinogen-binding genes (*fnAB*, etc.), were commonly upregulated in R5, R6, and MUP0.03 (Fig. 5a).

Most intriguingly, induction of the *ileS* gene, which encodes isoleucyl-tRNA synthetase (IleRS), was strongly upregulated in R3 and R6, similar to what was observed following mupirocin treatment. Although the *ileS* mutation was not detected as single nucleotide polymorphisms (SNPs) in R3 and R6, minor subpopulations with this gene mutation (D722N and G460A, respectively) were observed in both strains. In contrast, R5 and R6 induced the expression of the *leuS* gene, which encodes leucyl-tRNA synthetase (LeuRS) (Fig. 5a). Overexpression of *ileS* has been implicated in the activation of the global SR and induction of antibiotic tolerance after mupirocin treatment (26).

Validation of involvement of the SR in CPFX tolerance by qRT-PCR. The SR mediated by the global metabolic regulator (p)ppGpp often accounts for antibiotic tolerance and is induced under various stress conditions, including amino acid starvation and antibiotic exposure (28–30). Moreover, the SR can be endogenously induced following upregulation (29) or mutation of the GTP pyrophosphokinase genes *relA*, *relP*, and *relQ*, which have been termed SR genes (31, 32). In particular, *relA* mutations reportedly increase the levels of (p)ppGpp and induce beta-lactam resistance (33). Therefore, we suspect that RelA may be overactive in the R2 mutant, which acquired a nonsense mutation in the *relA* gene that could have resulted in deletion of the regulatory region, thereby causing the continuous synthesis of (p)ppGpp (25, 33). We found a marginal upregulation of the *relA* gene among the CPFX-tolerant and MUP0.03 strains using RNA-seq analysis (Table S1) and performed quantitative reverse transcription-PCR (qRT-PCR) to confirm this *relA* overexpression (Fig. 6). Interestingly, qRT-PCR showed that the *relA* gene was at least $\geq$2-fold ($P < 0.01$) upregulated in all of the CPFX-tolerant R strains, similar to the findings for MUP0.03 cells.

We also used qRT-PCR to confirm the changes in expression of genes encoding the amino acyl-tRNA synthetases (AARSs) IleRS and LeuRS (Fig. 6). Mupirocin is an IleRS inhibitor (34) and induces the global SR by accumulating uncharged isoleucine tRNA (tRNA-Ile) (28, 33). We accordingly confirmed, using RNA-seq (Table S1) and qRT-PCR (data not shown), the upregulation of *ileS* in MUP0.03, consistent with a previous report (26), as well as the similar upregulation of *ileS* in the R3 and R6 strains. In contrast, R5 and R6 showed the upregulation of *leuS*, another AARS gene, which was slightly downregulated in MUP0.03 and R3 cells but which remained unchanged in R2 (Fig. 6). Furthermore, the *ilvA* gene, located in the *ilv-leu* operon in the BCAA pathway, which is induced by the SR after mupirocin treatment (35), was also upregulated in R2, R5, and R6 (Table S1). Taken together, these results indicate that the SR is likely active in the R strains.

DISCUSSION

Bacterial tolerance to antibiotics is a major factor restricting the eradication of pathogens using antimicrobial therapy. Therefore, to develop new and effective antibiotic therapies, it is essential that we gain a fundamental understanding of the mechanisms responsible for the survival of bacteria in the presence of bactericidal antibiotics. Despite the fact that both the antibiotic tolerance and the antibiotic resistance of *S. aureus* have been known for over 70 years (17), we still understand much less about bacterial tolerance than we do about bacterial resistance. One reason for this is that, by definition, tolerant cells survive but do not grow in the presence of antibiotics (23, 36, 37), making it difficult to select tolerant bacteria. While many

Downloaded from https://journals.asm.org/journal/aac on 24 February 2022 by 2a01:4f9:3b:1ae9::

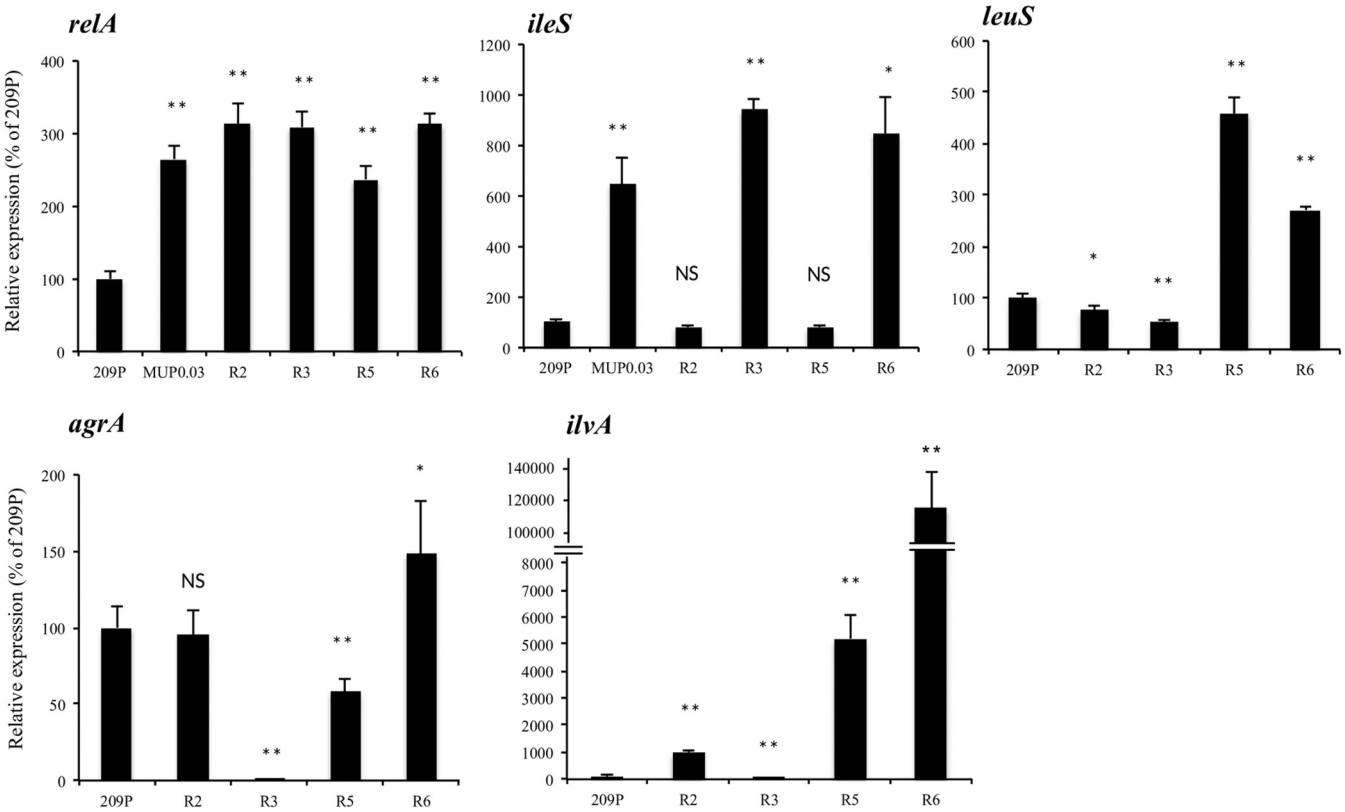

FIG 6 Verification of RNA-seq data by qRT-PCR. The relative expression of selected genes (*relA*, *ileS*, *leuS*, *ilvA*, and *agrA*) was determined by qRT-PCR in parent strain FDA209P, MUP0.03, and the CPFX-tolerant R strains. *dnaB* was used as the reference gene for normalization. Each bar represents the mean relative expression ± standard deviation for biological triplicates, where the mean expression in FDA209P is shown as 100%. Statistical significance was determined using Student's *t* test (*, $P < 0.05$; **, $P < 0.01$).

attempts have been made to develop methods to select tolerant cells in a heterogeneous population (11, 19–21), none of these can be used to routinely quantify the tolerance of a bacterial isolate in the clinic. Very recently, a method, called TDtest, which can easily detect antibiotic tolerance using a modified disk diffusion assay was described. However, this is a semiquantitative method and cannot be used to quantify the exact frequency of tolerant cells (38). A method for identifying tolerance based on the $MDK_{99.9}$ has also been proposed (11). While this method is suitable for use in research laboratories, it cannot be adopted for routine clinical testing due to the time and labor required to perform long-duration killing assays with multiple clinical isolates and different antibiotics.

In this study, we attempted to overcome these issues by developing a replica plating tolerance isolation system, named REPTIS, based on agar replica plating. We used this method to not only isolate but also calculate the frequency of tolerant cells and demonstrated that REPTIS is a simple, rapid, and fully quantitative method. Using REPTIS, we detected exceedingly low frequency cells with CPFX tolerance from the MSSA FDA209P strain (3.7×10^{-8}) and selected and established four strains (R2, R3, R5, and R6) whose tolerance phenotypes were confirmed (Fig. 1 and 2 and Tables 1 and 2). Phenotypic and whole-genome analyses revealed that these strains exhibited CPFX tolerance levels up to 100,000-fold higher than the tolerance level of the parent FDA209P strain (Fig. 2) and different mutation sets (Table 3). Tolerance did not require mutagenesis and appeared after only one CPFX exposure. Surprisingly, we observed that CPFX-tolerant mutants occurred at a rate of 10^{-8}, which was almost the same as that for resistance (2).

The CPFX-tolerant strains contained a number of notable mutations. The R2 strain carried a nonsense mutation in *relA*, R5 and R6 independently acquired the same single

Downloaded from https://journals.asm.org/journal/aac on 24 February 2022 by 2a01:4f9:3b:1ae9::

nucleotide polymorphism in the *leuS* gene, and R3 carried frameshift mutations in *mqo-2* (malate dehydrogenase) and an *ecsA* homolog (transportation). RelA senses amino acid starvation and synthesizes the stress alarmone (p)ppGpp, which reduces a bacterium's metabolic rate to enable survival under adverse conditions (29, 39). In previous studies, acquisition of *relA* mutations after antibiotic exposure induced beta-lactam tolerance in a (p)ppGpp-dependent manner (25, 32, 33). Similarly, the nonsense mutation at position 360 in *relA* may result in the deletion of the TGS (amino acids [aa] 402 to 461) and ACT (aa 661 to 727) domains. According to a previous report, deletion of the TGS and ACT domains in *relA* increases the synthesis of (p)ppGpp (33). The (p)ppGpp alarmone reprograms overall transcription either by directly binding to RNA polymerase (in Gram-negative bacteria) or by inhibiting global metabolic regulators, such as CodY (in Gram-positive bacteria) (40), thereby triggering the SR that results in global physiological changes (26, 41). A notable consequence of SR is the inactivation of pathways targeted by antibiotics, such as DNA replication and cell wall synthesis, leading to antibiotic tolerance due to the inactivation of antibiotic targets (23, 42). Here, we treated FDA209P cells with mupirocin, which induces the SR by accumulating uncharged tRNA-Ile by functionally inactivating the IleRS enzyme (26, 34, 43), to help determine whether CPFX tolerance occurs through the SR.

Physiological changes producing a state very similar to the SR state were observed in three of the four R strains when their transcriptomes were compared to the transcriptome of FDA209P treated with and without mupirocin (Fig. 3 to 5). Interestingly, the overall transcription pattern of mutants R2, R3, and R6 was similar to that of mupirocin-treated FDA209P (Fig. 3 and 4; see also Table S1 in the supplemental material). These strains also showed the induction of *relA*, as observed following mupirocin treatment (Fig. 6), supporting previous observations that *relA* upregulation can induce antibiotic tolerance (44, 45). Moreover, transcripts related to major cellular functions, such as translation (ribosomal genes), carbohydrate, fat, and energy metabolism, and nucleotide synthesis, were commonly downregulated, while amino acid biosynthesis- and transportation-related operons were upregulated in the R2, R3, and R6 strains, as in mupirocin-treated cells (Fig. 5). Moreover, the R strains used anaerobic respiration, as suggested from their common upregulation of the nitrate reductase genes (Table S1) and downregulation of the ATP synthase genes typical of aerobic respiration. Importantly, the anaerobic mode of respiration is preferred by virulent *S. aureus* bacteria during pathogenesis (27).

Recently, *ileS* gene upregulation was suggested to occur in the mupirocin-induced SR (26) due to the accumulation of uncharged tRNA-Ile (46). Notably, expression of *ileS* was increased in both the R3 and R6 strains, similar to what was observed under mupirocin treatment conditions (Fig. 6). A positive transcriptional relationship between the *ilv-leu* operon (encoding BCAA) and (p)ppGpp has been reported during the SR (35). Here, the R2, R5, and R6 strains all exhibited upregulation of the *ilv-leu* operon, although expression was unaltered in the R3 strain.

Based on the similar transcriptomics of R2, R3, and R6 with mupirocin-treated cells, we predict that CPFX tolerance involves the SR pathway in these strains. In the R2 strain, we hypothesize that the nonsense mutation in RelA, which lies at position 360, between the synthetase and regulatory domains, might result in deletion of the TGS and ACT domains while leaving synthetase activity intact. This would result in increased (p)ppGpp (33) due to the overactivity of RelA in the absence of an intact RSH regulatory region (25, 31). Meanwhile, the overexpression of *ileS* in R3 and R6 suggests induction of the RelA-dependent SR via accumulation of uncharged isoleucine tRNA (13, 26, 47). In addition, the R2, R3, and R6 mutants each carried a mutation that generated a premature stop codon in the SAFDA_2387, *mqo-2*, and *vga* genes, respectively. It is possible that these stop codons result in the functional impairment of these genes, potentially leading to an additive effect of the mutations in these strains, which could influence their tolerance.

In contrast to the other mutants and mupirocin-treated cells, a substantial induction of *leuS* was observed in R5, along with the upregulation of *relA* (Fig. 6). R5 carries an SNP

Downloaded from https://journals.asm.org/journal/aac on 24 February 2022 by 2a01:4f9:3b:1ae9::.

in *leuS* (R422C), and computational analysis suggested that this *leuS* mutation may have a significant impact on the stability of the LeuRS-Leu-tRNA^{Leu} complex (data not shown). This may cause a compensatory upregulation of the *leuS* gene due to leucine depletion and suggests that CPFX tolerance in R5 could also result from the accumulation of uncharged Leu-tRNA. Moreover, we did not observe induction of the *ileS* gene in R5, unlike the other R strains, nor did it show an overall transcription pattern similar to that in mupirocin-treated cells, suggesting that CPFX tolerance in R5 may not occur via an SR pathway that is initiated by uncharged Ile-tRNA. Furthermore, RNA sequencing revealed the common induction of virulence genes, such as *clfA* and *fnbA*, in mupirocin-treated cells and the R strains. However, R3 and R5 showed a marked downregulation of the *agrABCD* locus, which is a key virulence regulator. This was confirmed by the downregulation of *agrA* in these strains, observed using qRT-PCR (Fig. 6). Drug tolerance is a significant contributor to biofilm-associated infections by Gram-negative bacteria, especially *Pseudomonas aeruginosa* (21, 48). Therefore, our study may be useful for identifying such a strain before it develops overt resistance to colistin, the only available last-resort antibiotic. Moreover, these findings could also play a significant role in controlling the spread of antimicrobial resistance.

In summary, we successfully isolated four methicillin-sensitive *S. aureus* strains tolerant to CPFX using REPTIS. This method can be used to distinguish between tolerance and resistance. In addition to detecting antibiotic tolerance, this method can be used to quantify the frequency of tolerant cells in a subpopulation. Our study suggests that mutations for tolerance and resistance occur at the same frequency in *S. aureus*. The mutations in SR genes (*relA*) and AARSs (*ileS*, *leuS*) are likely key genetic determinants for antibiotic tolerance, including for tolerance to CPFX and vancomycin (unpublished data). The upregulation of *relA* may be a signature of tolerance driven by SR, and an ongoing study in our labs suggests that this may occur irrespective of antibiotic class (M. Singh, unpublished data). Combined genomic and transcriptome analyses demonstrated that CPFX tolerance in these four *S. aureus* mutants occurred via at least two distinct mechanisms: (i) a mechanism similar to that for tolerance to mupirocin (R2, R3 and R6) via uncharged Ile-tRNA pathways and (ii) a mechanism different from that for tolerance to mupirocin (R5) via uncharged Leu-tRNA pathways.

MATERIALS AND METHODS

Selection of ciprofloxacin-tolerant strains. The standard MSSA strain FDA209P was used for the selection of CPFX-tolerant strains using the REPTIS method. Briefly, approximately 10^8 CFU of the FDA209P strain was exposed to 1 mg/liter (15-fold the MIC) CPFX on a brain heart infusion (BHI) agar plate (master plate). After 72 h of incubation, the colonies from the master plate (which were nongrowing due to the drug) were transferred onto a drug-free BHI agar plate (replica plate), and the ratio of the number of colonies surviving in the presence of CPFX to the total number of colonies was measured after 72 h of incubation on the replica plate. A total of four selected CPFX-tolerant colonies were purified for further genotypic and phenotypic analyses.

Antibiotic susceptibility. The MIC of CPFX was determined using the Etest (AB Biodisk, Solna, Sweden) method on BHI agar medium, according to the manufacturer's instructions. The MIC was recorded after 24 and 48 h of incubation.

Time-kill assay. Stationary-phase cultures of all four CPFX-tolerant mutants and the FDA209P parent strain were inoculated in tryptic soy broth (TSB) (final cell density, 10^5 CFU/ml) containing 1 mg/liter CPFX (15-fold the MIC, because the MIC value of FDA209P was 0.064 mg/liter) and incubated at 37°C with shaking. A 100-μl aliquot of each culture was harvested at the indicated time points (0, 3, 6, and 24 h), diluted in saline, and plated onto TSB agar. Viable colonies were counted after 72 h of incubation at 37°C. Killing data are presented as the mean $\pm$ standard deviation (SD) from three independent experiments.

Whole-genome sequencing. Genomic DNA was isolated using a Qiagen QIAamp DNA minikit (Qiagen Inc., Valencia, CA). A DNA library was prepared using a Nextera XT DNA sample preparation kit (Illumina, Inc., San Diego, CA). The normalized DNA library was sequenced on an Illumina MiSeq next-generation sequencing platform (Illumina. Inc., San Diego, CA), and 250-bp end reads were generated. The sequence reads were mapped to the whole-genome reference sequence of the FDA209P strain (GenBank accession no. AP014942) (49). The average percentage of reads mapped to the reference genome was 99.94%. Mutations, including SNPs, insertions, and deletions, were identified using the CLC Genomics Workbench, and each of the detected mutations was confirmed by Sanger sequencing.

RNA sequencing data analysis and statistics. Total RNA was isolated from bacterial cultures grown to mid-exponential phase at 37°C, using an RNeasy minikit (Qiagen), according to the manufacturer's instructions. The quality of the total RNA was confirmed using an Agilent 2100 bioanalyzer. Illumina

Downloaded from https://journals.asm.org/journal/aac on 24 February 2022 by 2a01:4f9:3b:1ae9::

TABLE 4 List of primers used for qRT-PCR

Target gene	Sequence (5′ → 3′)	
	Forward primer	Reverse primer
dnaB	GCCGATATCGTTGCATTCTT	GTTGGACCGTTACGTTGCTT
relA	ATTAGACGGACCGACGATTG	TTGCGATGATTTTCAGCTTG
ileS	GGAACCGCAAATTCAAGAAA	ATGGTGCATAGAACCCTTGC
leuS	GCGAACCAATTCCTGTCATT	TGTTTCACGACGTCCTTTCA
ilvA	TATTTGCCGCTATTGGTGGT	CTACAGATGCACCGTCCACA
agrA	AATTGCCCTCGCAACTGATA	TGTTACCAACTGGGTCATGC

sequencing of cDNA (Illumina RNA-seq) was performed for comparative transcriptomic analysis of the R strains versus untreated FDA209P and FDA209P treated with mupirocin. Sequencing was performed using a paired-end 2 × 100-bp cycle run on an Illumina HiSeq 2500 sequencing system. Read counts were summarized against the FDA209P reference genomes (GenBank accession no. AP014942 and AP014943) (49) using the feature Counts (50). Differential gene expression analysis was performed using the edgeR package (51), which identifies genes with significant differences in expression from genome-scale count data using exact tests based on the negative binomial distribution. Reads that were mapped to multiple locations in an open reading frame (ORF) or to multiple ORFs were discarded using SAMtools (52). The raw read counts were normalized using the iDEGES/edgeR method (53), and pairwise comparisons of digital gene expression between each mutant and the FDA209P parent strain treated or not treated with mupirocin were conducted using the edgeR program in R (51). False discovery rate (FDR) adjustments (54) were applied to correct for multiple testing, and differentially expressed genes were identified using an FDR threshold of 0.05. For PCA, the raw reads were filtered and trimmed by removing bases with quality value scores of 20 or less and read lengths shorter than 50 bases using the Cutadapt and Trimmomatic programs. Read mapping against the FDA209P reference genome was performed using the TopHat program (55). This yielded the number of fragments per kilobase of transcript per million mapped fragments (FPKM) value, which was used for PCA. PCA was repeated in triplicate for assessment of reproducibility (see Fig. S2 in the supplemental material).

qRT-PCR. Five hundred nanograms of total RNA was reverse transcribed to cDNA using SuperScript IV Vilo master mix (Invitrogen by Thermo Fisher Scientific) according to the manufacturer's protocol. Real-time PCR assays were performed using a PowerUp SYBR Green master mix kit (Thermo Fisher Scientific, Carlsbad, CA, USA) with the primer sets for *dnaB*, *relA*, *ileS*, and *leuS* (Table 4). Thermocycler conditions for real-time PCR consisted of an initial denaturation at 95°C for 20 s and 40 cycles of 95°C for 1 s and 60°C for 20 s. Data were collected using the QuantStudio 3 system (Thermo Fisher Scientific, Carlsbad, CA, USA). For relative quantification, cycle threshold (C_T) values were used to calculate fold changes in expression using the $2^{-\Delta\Delta CT}$ method and the *dnaB* gene as a reference for normalization. Each bar represents the mean relative expression ± standard deviation for biological triplicates, where the mean expression in FDA209P is shown as 100%. Statistical significance was determined using Student's *t* test.

SUPPLEMENTAL MATERIAL

Supplemental material for this article may be found at https://doi.org/10.1128/AAC.02019-18.

SUPPLEMENTAL FILE 1, PDF file, 0.7 MB.

SUPPLEMENTAL FILE 2, XLSX file, 0.2 MB.

ACKNOWLEDGMENTS

This study was supported by grant-in-aid S1201013 from the Japanese Ministry of Education, Culture, Sports, Science and Technology (MEXT)-Supported Program for the Strategic Research Foundation at Private Universities, 2012 to 2017. M.S. thanks CSIR-India for a senior research associateship.

REFERENCES

1. Fasugba O, Gardner A, Mitchell BG, Mnatzaganian G. 2015. Ciprofloxacin resistance in community- and hospital-acquired Escherichia coli urinary tract infections: a systematic review and meta-analysis of observational studies. BMC Infect Dis 15:545. https://doi.org/10.1186/s12879-015-1282-4.
2. Hiramatsu K, Igarashi M, Morimoto Y, Baba T, Umekita M, Akamatsu Y. 2012. Curing bacteria of antibiotic resistance: reverse antibiotics, a novel class of antibiotics in nature. Int J Antimicrob Agents 39:478–485. https://doi.org/10.1016/j.ijantimicag.2012.02.007.
3. Hiramatsu K, Katayama Y, Matsuo M, Sasaki T, Morimoto Y, Sekiguchi A, Baba T. 2014. Multi-drug-resistant Staphylococcus aureus and future chemotherapy. J Infect Chemother 20:593–601. https://doi.org/10.1016/j.jiac.2014.08.001.
4. Blumberg HM, Rimland D, Carroll DJ, Terry P, Wachsmuth IK. 1991. Rapid development of ciprofloxacin resistance in methicillin-susceptible and -resistant Staphylococcus aureus. J Infect Dis 163:1279–1285. https://doi.org/10.1093/infdis/163.6.1279.
5. Sreedharan S, Peterson LR, Fisher LM. 1991. Ciprofloxacin resistance in

Downloaded from https://journals.asm.org/journal/aac on 24 February 2022 by 2a01:4f9:3b:1ae9::

coagulase-positive and -negative staphylococci: role of mutations at serine 84 in the DNA gyrase A protein of Staphylococcus aureus and Staphylococcus epidermidis. Antimicrob Agents Chemother 35: 2151–2154. https://doi.org/10.1128/AAC.35.10.2151.
6. Hori S, Ohshita Y, Utsui Y, Hiramatsu K. 1993. Sequential acquisition of norfloxacin and ofloxacin resistance by methicillin-resistant and -susceptible Staphylococcus aureus. Antimicrob Agents Chemother 37: 2278–2284. https://doi.org/10.1128/AAC.37.11.2278.
7. Yoshida H, Bogaki M, Nakamura S, Ubukata K, Konno M. 1990. Nucleotide sequence and characterization of the Staphylococcus aureus norA gene, which confers resistance to quinolones. J Bacteriol 172: 6942–6949. https://doi.org/10.1128/jb.172.12.6942-6949.1990.
8. Conlon BP, Rowe SE, Gandt AB, Nuxoll AS, Donegan NP, Zalis EA, Clair G, Adkins JN, Cheung AL, Lewis K. 2016. Persister formation in Staphylococcus aureus is associated with ATP depletion. Nat Microbiol 1:16051. https://doi.org/10.1038/nmicrobiol.2016.51.
9. Kester JC, Fortune SM. 2014. Persisters and beyond: mechanisms of phenotypic drug resistance and drug tolerance in bacteria. Crit Rev Biochem Mol Biol 49:91–101. https://doi.org/10.3109/10409238.2013.869543.
10. Hiramatsu K, Kayayama Y, Matsuo M, Aiba Y, Saito M, Hishinuma T, Iwamoto A. 2014. Vancomycin-intermediate resistance in Staphylococcus aureus. J Glob Antimicrob Resist 2:213–224. https://doi.org/10.1016/j.jgar.2014.04.006.
11. Brauner A, Fridman O, Gefen O, Balaban NQ. 2016. Distinguishing between resistance, tolerance and persistence to antibiotic treatment. Nat Rev Microbiol 14:320–330. https://doi.org/10.1038/nrmicro.2016.34.
12. Mechler L, Bonetti EJ, Reichert S, Flotenmeyer M, Schrenzel J, Bertram R, Francois P, Gotz F. 2016. Daptomycin tolerance in the Staphylococcus aureus pitA6 mutant is due to upregulation of the dlt operon. Antimicrob Agents Chemother 60:2684–2691. https://doi.org/10.1128/AAC.03022-15.
13. Singh M, Matsuo M, Sasaki T, Morimoto Y, Hishinuma T, Hiramatsu K. 2016. In vitro tolerance of drug-naive Staphylococcus aureus strain FDA209P to vancomycin. Antimicrob Agents Chemother 61:e01154-16. https://doi.org/10.1128/AAC.01154-16.
14. Tuomanen E, Durack DT, Tomasz A. 1986. Antibiotic tolerance among clinical isolates of bacteria. Antimicrob Agents Chemother 30:521–527. https://doi.org/10.1128/AAC.30.4.521.
15. Lewis K. 2010. Persister cells. Annu Rev Microbiol 64:357–372. https://doi.org/10.1146/annurev.micro.112408.134306.
16. Fisher RA, Gollan B, Helaine S. 2017. Persistent bacterial infections and persister cells. Nat Rev Microbiol 15:453. https://doi.org/10.1038/nrmicro.2017.42.
17. Bigger J. 1944. Treatment of staphylococcal infections with penicillin by intermittent sterilisation. Lancet 244:497–500. https://doi.org/10.1016/S0140-6736(00)74210-3.
18. Levin-Reisman I, Ronin I, Gefen O, Braniss I, Shoresh N, Balaban NQ. 2017. Antibiotic tolerance facilitates the evolution of resistance. Science 355: 826–830. https://doi.org/10.1126/science.aaj2191.
19. Babin BM, Atangcho L, van Eldijk MB, Sweredoski MJ, Moradian A, Hess S, Tolker-Nielsen T, Newman DK, Tirrell DA. 2017. Selective proteomic analysis of antibiotic-tolerant cellular subpopulations in Pseudomonas aeruginosa biofilms. mBio 8:e01593-17. https://doi.org/10.1128/mBio.01593-17.
20. Brauner A, Shoresh N, Fridman O, Balaban NQ. 2017. An experimental framework for quantifying bacterial tolerance. Biophys J 112:2664–2671. https://doi.org/10.1016/j.bpj.2017.05.014.
21. Chua SL, Yam JKH, Hao P, Adav SS, Salido MM, Liu Y, Givskov M, Sze SK, Tolker-Nielsen T, Yang L. 2016. Selective labelling and eradication of antibiotic-tolerant bacterial populations in Pseudomonas aeruginosa biofilms. Nat Commun 7:10750. https://doi.org/10.1038/ncomms10750.
22. Fridman O, Goldberg A, Ronin I, Shoresh N, Balaban NQ. 2014. Optimization of lag time underlies antibiotic tolerance in evolved bacterial populations. Nature 513:418–421. https://doi.org/10.1038/nature13469.
23. Gefen O, Balaban NQ. 2009. The importance of being persistent: heterogeneity of bacterial populations under antibiotic stress. FEMS Microbiol Rev 33:704–717. https://doi.org/10.1111/j.1574-6976.2008.00156.x.
24. Tuomanen E, Cozens R, Tosch W, Zak O, Tomasz A. 1986. The rate of killing of Escherichia coli by beta-lactam antibiotics is strictly proportional to the rate of bacterial growth. J Gen Microbiol 132:1297–1304. https://doi.org/10.1099/00221287-132-5-1297.
25. Hogg T, Mechold U, Malke H, Cashel M, Hilgenfeld R. 2004. Conformational antagonism between opposing active sites in a bifunctional RelA/SpoT homolog modulates (p)ppGpp metabolism during the stringent response. Cell 117:57–68. https://doi.org/10.1016/S0092-8674(04)00260-0.
26. Reiß S, Pané-Farré J, Fuchs S, François P, Liebeke M, Schrenzel J, Lindequist U, Lalk M, Wolz C, Hecker M. 2011. Global analysis of the Staphylococcus aureus response to mupirocin. Antimicrob Agents Chemother 56:787–804. https://doi.org/10.1128/AAC.05363-11.
27. Chaffin DO, Taylor D, Skerrett SJ, Rubens CE. 2012. Changes in the Staphylococcus aureus transcriptome during early adaptation to the lung. PLoS One 7:e41329. https://doi.org/10.1371/journal.pone.0041329.
28. Traxler MF, Summers SM, Nguyen HT, Zacharia VM, Hightower GA, Smith JT, Conway T. 2008. The global, ppGpp-mediated stringent response to amino acid starvation in Escherichia coli. Mol Microbiol 68:1128–1148. https://doi.org/10.1111/j.1365-2958.2008.06229.x.
29. Geiger T, Goerke C, Fritz M, Schäfer T, Ohlsen K, Liebeke M, Lalk M, Wolz C. 2010. Role of the (p)ppGpp synthase RSH, a RelA/SpoT homolog, in stringent response and virulence of Staphylococcus aureus. Infect Immun 78:1873–1883. https://doi.org/10.1128/IAI.01439-09.
30. Dalebroux ZD, Swanson MS. 2012. ppGpp: magic beyond RNA polymerase. Nat Rev Microbiol 10:203–212. https://doi.org/10.1038/nrmicro2720.
31. Gao W, Chua K, Davies JK, Newton HJ, Seemann T, Harrison PF, Holmes NE, Rhee H-W, Hong J-I, Hartland EL, Stinear TP, Howden BP. 2010. Two novel point mutations in clinical Staphylococcus aureus reduce linezolid susceptibility and switch on the stringent response to promote persistent infection. PLoS Pathog 6:e1000944. https://doi.org/10.1371/journal.ppat.1000944.
32. Honsa ES, Cooper VS, Mhaissen MN, Frank M, Shaker J, Iverson A, Rubnitz J, Hayden RT, Lee RE, Rock CO. 2017. RelA mutant Enterococcus faecium with multiantibiotic tolerance arising in an immunocompromised host. mBio 8:e02124-16. https://doi.org/10.1128/mBio.02124-16.
33. Mwangi MM, Kim C, Chung M, Tsai J, Vijayadamodar G, Benitez M, Jarvie TP, Du L, Tomasz A. 2013. Whole-genome sequencing reveals a link between beta-lactam resistance and synthetases of the alarmone (p)ppGpp in Staphylococcus aureus. Microb Drug Resist 19:153–159. https://doi.org/10.1089/mdr.2013.0053.
34. Nakama T, Nureki O, Yokoyama S. 2001. Structural basis for the recognition of isoleucyl-adenylate and an antibiotic, mupirocin, by isoleucyl-tRNA synthetase. J Biol Chem 276:47387–47393. https://doi.org/10.1074/jbc.M109089200.
35. Tojo S, Satomura T, Kumamoto K, Hirooka K, Fujita Y. 2008. Molecular mechanisms underlying the positive stringent response of the Bacillus subtilis ilv-leu operon, involved in the biosynthesis of branched-chain amino acids. J Bacteriol 190:6134–6147. https://doi.org/10.1128/JB.00606-08.
36. Gilbert P, Collier PJ, Brown MR. 1990. Influence of growth rate on susceptibility to antimicrobial agents: biofilms, cell cycle, dormancy, and stringent response. Antimicrob Agents Chemother 34: 1865–1868. https://doi.org/10.1128/AAC.34.10.1865.
37. Shah D, Zhang Z, Khodursky A, Kaldalu N, Kurg K, Lewis K. 2006. Persisters: a distinct physiological state of E. coli. BMC Microbiol 6:53. https://doi.org/10.1186/1471-2180-6-53.
38. Gefen O, Chekol B, Strahilevitz J, Balaban NQ. 2017. TDtest: easy detection of bacterial tolerance and persistence in clinical isolates by a modified disk-diffusion assay. Sci Rep 7:41284. https://doi.org/10.1038/srep41284.
39. Geiger T, Kastle B, Gratani FL, Goerke C, Wolz C. 2014. Two small (p)ppGpp synthases in Staphylococcus aureus mediate tolerance against cell envelope stress conditions. J Bacteriol 196:894–902. https://doi.org/10.1128/JB.01201-13.
40. Gaca AO, Colomer-Winter C, Lemos JA. 2015. Many means to a common end: the intricacies of (p)ppGpp metabolism and its control of bacterial homeostasis. J Bacteriol 197:1146–1156. https://doi.org/10.1128/JB.02577-14.
41. Nazir A, Harinarayanan R. 2016. (p)ppGpp and the bacterial cell cycle. J Biosci 41:277–282. https://doi.org/10.1007/s12038-016-9611-3.
42. Corrigan RM, Bellows LE, Wood A, Gründling A. 2016. ppGpp negatively impacts ribosome assembly affecting growth and antimicrobial tolerance in Gram-positive bacteria. Proc Natl Acad Sci U S A 113: E1710–E1719. https://doi.org/10.1073/pnas.1522179113.
43. Eymann C, Homuth G, Scharf C, Hecker M. 2002. Bacillus subtilis functional genomics: global characterization of the stringent response by proteome and transcriptome analysis. J Bacteriol 184:2500–2520. https://doi.org/10.1128/JB.184.9.2500-2520.2002.
44. Abranches J, Martinez AR, Kajfasz JK, Chavez V, Garsin DA, Lemos JA.

Downloaded from https://journals.asm.org/journal/aac on 24 February 2022 by 2a01:4f9:3b:1ae9::

2009. The molecular alarmone (p)ppGpp mediates stress responses, vancomycin tolerance, and virulence in Enterococcus faecalis. J Bacteriol 191:2248–2256. https://doi.org/10.1128/JB.01726-08.
45. Kudrin P, Varik V, Oliveira SRA, Beljantseva J, Santos TDP, Dzhygyr I, Rejman D, Cava F, Tenson T, Hauryliuk V. 2017. Subinhibitory concentrations of bacteriostatic antibiotics induce relA-dependent and relA-independent tolerance to β-lactams. Antimicrob Agents Chemother 61:02173-16. https://doi.org/10.1128/AAC.02173-16.
46. Silvian LF, Wang J, Steitz TA. 1999. Insights into editing from an ile-tRNA synthetase structure with tRNAile and mupirocin. Science 285: 1074–1077. https://doi.org/10.1126/science.285.5430.1074.
47. Iaccarino M, Berg P. 1971. Isoleucine auxotrophy as a consequence of a mutationally altered isoleucyl-transfer ribonucleic acid synthetase. J Bacteriol 105:527–537.
48. Lewis K. 2008. Multidrug tolerance of biofilms and persister cells, p 107–131. *In* Bacterial biofilms. Springer, New York, NY.
49. Singh M, Sasaki T, Matsuo M, Morimoto Y, Aiba Y, Hiramatsu K. 2015. Complete genome sequence of the drug-naive classical Staphylococcus aureus strain FDA209P. Genome Announc 3(6):e01343-15. https://doi.org/10.1128/genomeA.01343-15.
50. Liao Y, Smyth GK, Shi W. 2014. featureCounts: an efficient general purpose program for assigning sequence reads to genomic features. Bioinformatics 30:923–930. https://doi.org/10.1093/bioinformatics/btt656.
51. Robinson MD, McCarthy DJ, Smyth GK. 2010. edgeR: a Bioconductor package for differential expression analysis of digital gene expression data. Bioinformatics 26:139–140. https://doi.org/10.1093/bioinformatics/btp616.
52. Li H, Handsaker B, Wysoker A, Fennell T, Ruan J, Homer N, Marth G, Abecasis G, Durbin R. 2009. The sequence alignment/map format and SAMtools. Bioinformatics 25:2078–2079. https://doi.org/10.1093/bioinformatics/btp352.
53. Sun J, Nishiyama T, Shimizu K, Kadota K. 2013. TCC: an R package for comparing tag count data with robust normalization strategies. BMC Bioinformatics 14:219. https://doi.org/10.1186/1471-2105-14-219.
54. Benjamini Y, Hochberg Y. 1995. Controlling the false discovery rate: a practical and powerful approach to multiple testing. J R Stat Soc Series B Stat Methodol 57:289–300.
55. Trapnell C, Pachter L, Salzberg SL. 2009. TopHat: discovering splice junctions with RNA-Seq. Bioinformatics 25:1105–1111. https://doi.org/10.1093/bioinformatics/btp120.

Downloaded from https://journals.asm.org/journal/aac on 24 February 2022 by 2a01:4f9:3b:1ae9::.